Biointerface Research in Applied Chemistry
Open-Access Journal (ISSN: 2069-5837)

Article
Volume 16, Issue 1, 2026, 15
https://doi.org/10.33263/BRIAC161.015

Receptor-Guided Screening of Marine Bioactive Compounds as Potential Allosteric SHP2 Inhibitors

Pracheta Singh [1], Swadesh Kumar Pattanik [1,*], Jeevan Patra [1]

[1] Department of Pharmaceutical Chemistry, Amity Institute of Pharmacy, Amity University Uttar Pradesh, Lucknow Campus, Lucknow - 226028, Uttar Pradesh, India
* Correspondence: skpattanik@lko.amity.edu;

Received: 15.09.2025; Accepted: 29.10.2025; Published: 15.02.2026

Abstract: The development of effective cancer therapeutics remains a major challenge due to substantial adverse effects, poor efficacy, modest pharmacokinetic profiles, and limited selectivity. Thus, identifying novel chemotypes against key oncogenic targets is imperative. Src homology 2 domain-containing phosphatase 2 (SHP2), encoded by the protein tyrosine phosphatase non-receptor type 11 (PTPN11) gene, controls cellular processes such as proliferation, differentiation, apoptosis, and survival through tyrosine dephosphorylation. Marine bioactive compounds offer distinctive chemical scaffolds that are valuable for anticancer drug discovery. In this study, the Comprehensive Marine Natural Product Database (CMNPD) was explored to identify potential marine bioactives targeting the allosteric site of SHP2 through integrated computational analyses, including structure-guided pharmacophore modeling, docking, and molecular dynamics (MD) simulations. Three lead candidates — *CMNPD23791* (Hyrtioerectine E), *CMNPD15129* (Hyrtioerectine A), and *CMNPD25856* (pre-pseudomonine) — have higher binding affinities (-54.9 kcal/mol, -58.2 kcal/mol, and -53.3 kcal/mol, respectively) compared with the reference *SHP099* (-39.08 kcal/mol). Moreover, these hits demonstrated favorable interactions at the allosteric tunnel cavity and desirable drug-likeness properties. Molecular dynamics simulations (100 ns) confirmed stable complexes with average root mean square deviation (RMSD) below 1.4 Å and consistent compactness (Rg 17.6 Å – 17.7 Å). These findings suggest that the identified marine compounds could serve as promising allosteric SHP2 inhibitors and provide a basis for further experimental validation of marine SHP2 inhibitors.

Keywords: cancer; SHP2; allosteric inhibitors; marine compounds; binding affinity.

1. Introduction

Src homology-2-containing protein tyrosine phosphatase (SHP2), encoded by the PTPN11 gene, is a non-receptor protein tyrosine phosphatase crucial for cell proliferation, differentiation, migration, metabolism, and survival [1,2]. It functions through reversible tyrosine dephosphorylation and plays a pivotal role in oncogenic receptor tyrosine kinase (RTK) signaling [3,4]. Dysregulated SHP2 activity has strong implications in solid tumors, including melanoma, esophageal squamous cell carcinoma, lung, and liver cancers [5,6].

Traditional SHP2 inhibitors such as *NSC-87877* [7], *PHPS1* [8], and *NAT6-297775* [9] targeted the catalytic PTP domain but lacked selectivity and clinical efficacy. Novartis Pharmaceuticals boosted the discovery of an allosteric inhibitor, *SHP099* [10], which stabilizes

SHP2's inactive conformation by occupying the tunnel site between the N-SH2 and PTP domains, leading to significant therapeutic advances. Several *SHP099* derivatives, such as *TNO155* [11], *JAB-3068* [12], *RLY-1971* (*GDC-1971*) [13], and *ARRY-558* [14] have advanced into clinical phases; however, limited therapeutic benefits and resistance persist [15]. Hence, these challenges highlight the need for novel allosteric chemotypes that can improve efficacy.

Natural bioactive molecules from marine sources have been an invaluable resource for the discovery of cancer drugs, owing to their structural diversity and evolutionary optimization [16]. Marine organisms—sponges, algae, ascidians, and microorganisms produce metabolites with unique scaffolds and potent bioactivities, offering opportunities to identify new SHP2 inhibitors [17,18]. Structure-based virtual screening and pharmacophore modeling are widely adopted strategies in the early-stage drug discovery to identify lead candidates from large chemical libraries [19,20]. These computational approaches provide an efficient and rational framework for discovering potent inhibitors and predicting their molecular interactions and stability before experimental validation.

Despite significant advances in SHP2 allosteric inhibitor discovery, most reported studies have focused on *SHP099*-derived analogs. However, very few investigations have explored natural product scaffolds as potential allosteric SHP2 inhibitors [21,22]. To the best of our knowledge, no study has reported on marine bioactives using computational methods. This gap limits the understanding of how marine chemotypes could modulate the SHP2 allosteric mechanism.

Hence, we set out to bridge this gap by employing receptor-guided, pharmacophore-based screening of marine compounds to identify novel, structurally distinct SHP2 inhibitors. In this study, we systematically explored the Comprehensive Marine Natural Product Database (CMNPD) using an integrated computational workflow combining receptor-guided pharmacophore modeling, molecular docking, molecular mechanics- Poisson- Boltzmann surface area (MM- PBSA) free energy estimation, and molecular dynamics simulations.

2. Materials and Methods

The overall computational workflow adopted in this study is summarized in Figure 1.

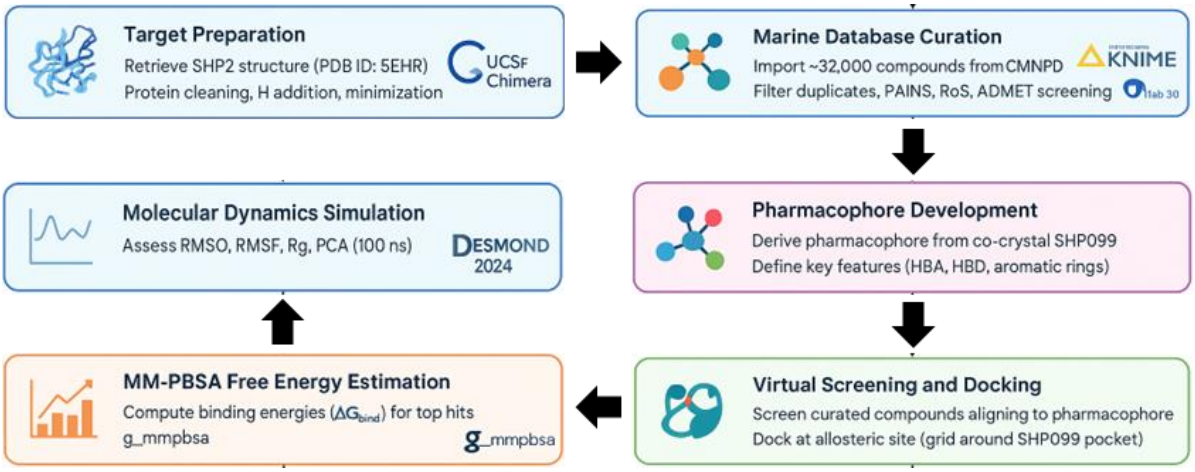

Figure 1. Schematic workflow illustrating the integrated computational pipeline used for identifying potential allosteric SHP2 inhibitors from marine natural products.

2.1. Structural crystallography preparation.

The crystallographic structure of allosterically bound SHP2 complex (PDB ID: 5EHR) [10], resolved at a 1.70 Å resolution, was retrieved from the RCSB protein data bank (PDB).

Non-essential crystallographic components, including heteroatoms, cofactors, and solvent molecules, were removed. The protein structure was examined for missing loops, and hydrogen atoms were added to ensure proper protonation. Kollmann charges were assigned, and the system was energy-minimized in Chimera to obtain a relaxed, stable conformation for subsequent modeling studies.

2.2. Marine virtual database and ligand preparation.

A marine product database containing 32,000 molecules was retrieved from the Comprehensive Marine Natural Products Database (CMNPD) [23]. Duplicate entries and ambiguous chemical structures were removed using the RDKit and KNIME workflow platforms. The resulting unique compounds were further screened for pan-assay interference (PAINS) compounds, compliance with the Lipinski rule of five (Ro5), and pharmacokinetic properties using ADMETLab 3.0 [24]. This multistage screening produced 4,926 bioactive compounds suitable for downstream pharmacophore-based screening. The qualified marine compounds were optimized using the SQM program with AM1-BCC and the UCSF Chimera Prep module.

2.3. Pharmacophore development and screening.

The receptor-guided pharmacophore model of SHP2 was developed using Pharmit (https://pharmit.csb.pitt.edu/) [25]. The pharmacophore features, such as hydrogen bond donor, hydrogen bond acceptor, hydrophobic, positive, negative, and aromatic ring of the co-crystal, were considered for screening. The curated marine databases were screened to assess the alignment score (RMSD, Å), which could interact with the key binding residues similar to those of the co-crystal.

2.4. Receptor grid generation, molecular docking, and MM-PBSA estimation.

MzDOCK is an integrated GUI-based pipeline that computes using MMFF94s force field, thus providing accurate and reliable docking poses while comparing with any standard [26]. The grid was centered on the co-crystallized ligand to generate a three-dimensional grid box surrounding residues within 4.0 Å. The docking validation with the co-crystal and best pharmacophore-aligned marine hits was performed using the default parameters of MzDOCK. Following the docking execution, the molecular interactions were produced using PyMOL.

The absolute binding free energy (ΔG_{bind}) of the top docked complexes was estimated using the MM-PBSA method implemented in the g_mmpbsa package [27] using the MMFF94s force field. The last 20 ns trajectory of the 100 ns MD simulation was used for free energy calculations, and 500 evenly spaced frames were extracted from this segment for MM-PBSA analysis.

2.4. Molecular dynamics simulations.

Molecular dynamics simulations of all complexes were performed using Desmond academic version 2024 [28] to evaluate structural stability and conformational flexibility of SHP2-marine bioactive complexes. The best-docked conformers were solvated using the TIP5P explicit water model truncated in an orthorhombic box extending 10 Å in all directions. The systems were neutralized with 0.15 M NaCl physiological salts. Energy minimization was performed using the steepest descent algorithm until a gradient threshold of 25 kcal/mol/Å was

reached. The non-bonded interaction cut-off distance for coulombic and van der Waals forces was set to 9.0 Å, and long-range electrostatics were treated using the Particle Mesh Ewald (PME) method. A dielectric constant of 1.0 was applied to the system for non-bonded interactions. Subsequently, each system was equilibrated under isothermal-isobaric (NPT) ensemble conditions at a temperature of 300 K and pressure of 1.013 bar using the Nose-Hoover thermostat and Martyna-Tobias-Klein barostat. The time step was set to 2 fs, and the trajectories were simulated for 100 ns under the OPLS4 force field.

3. Results and Discussion

3.1. Development of pharmacophore model and screening.

The receptor-guided pharmacophore model of the SHP2 complex was developed based on crystallographic evidence to identify key interactions within the allosteric binding site (Figure 2). The pharmacophoric features—hydrogen bond donor (HBD), hydrogen bond acceptor (HBA), hydrophobic group (H), positive ionizable (P), negative ionizable (N), and aromatic ring (R)— were derived from the co-crystallized ligand and its interactions with critical amino acid residues. Screening marine compounds that align with these features was expected to reproduce a binding pattern similar to that of the co-crystal.

The final SHP2 pharmacophore model consisted of five essential features: two aromatic rings, two hydrogen bond donors, and one hydrogen bond acceptor. The *1,2-dichlorophenyl* ring formed a π-cation interaction (colored in dark green) with Arg111 residue and a halogen interaction (colored in dark brown) with Thr253 residue. The *2-aminopyrazine* moiety established hydrogen bonds (colored in magenta) with Arg111 and Glu250 residues, while the amino-cyclohexane group displayed electrostatic interaction (colored in black), and hydrogen bonding with Glu249 and His114, along with a π-cation interaction with Phe113 residue. These combined interactions defined the essential pharmacophoric elements required for allosteric inhibition of SHP2.

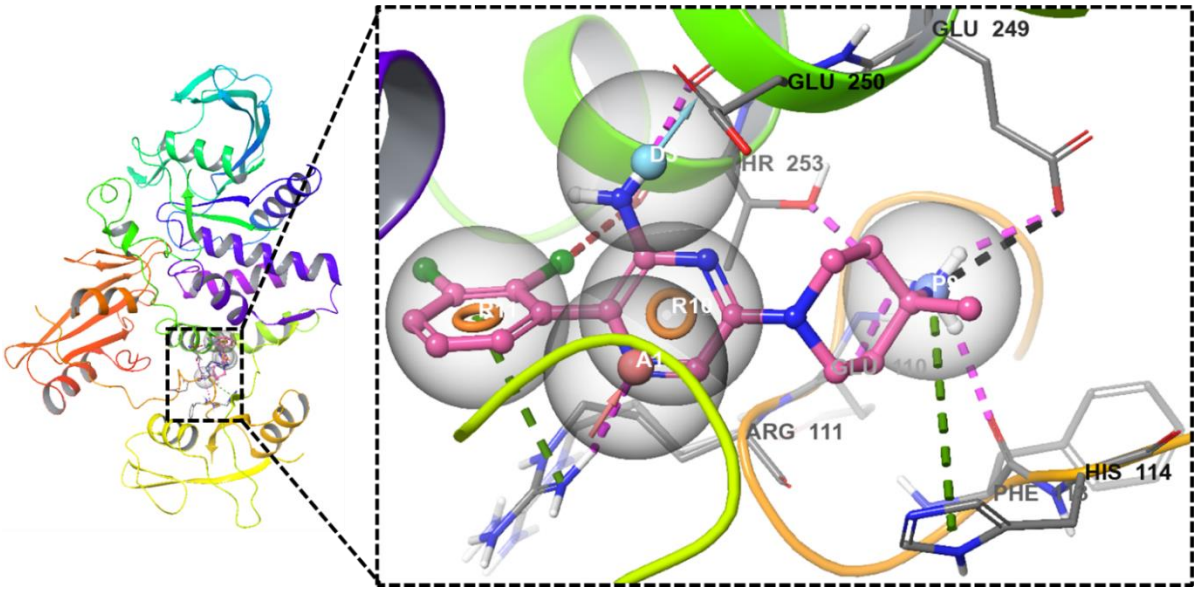

Figure 2. Receptor-guided pharmacophore model of SHP2 complexed with co-crystal *SHP099* (colored in magenta). Here, the pharmacophore features such as aromatic rings, hydrophobic, hydrogen bond acceptor, and hydrogen bond donors are colored in orange, green, red, and violet. The hydrogen bond, halogen interaction, π-π stacking, and electrostatic interaction are in dashed lines and colored in pink, brown, dark green, and black, respectively.

Pharmacophore-based virtual screening of the marine compound library was performed to identify molecules that aligned with the key interaction features defined in the SHP2 pharmacophore model, with a root mean square deviation (RMSD) below 2.0 Å. The initial screening yielded 887 compounds that satisfied all five pharmacophoric features. These compounds displayed diverse alignment scores. To refine the results, the dataset was further filtered by alignment score, yielding 121 promising marine hits. These shortlisted compounds were subsequently evaluated by molecular docking to assess their binding affinities and identify potential allosteric SHP2 inhibitors.

3.2. Marine compounds interacted at the allosteric SHP2 pocket.

To validate the docking protocol, the co-crystallized ligand (*SHP099*) was re-docked into its native allosteric binding pocket with identical grid parameters and docking constraints. The root mean square deviation (RMSD) between the experimental (co-crystal) and re-docked pose was 0.42 Å, indicating a good superposition and confirming the reliability of the docking protocol (Figure S1). The re-docked *SHP099* also exhibited a comparable binding score of -4.987 kcal/mol, and the corresponding molecular mechanics Poisson–Boltzmann surface area (MM-PBSA) was -39.08 kcal/mol. The key binding interactions with Glu110, Arg111, Phe113, His114, Glu249, Glu250, and Thr253 residues, cconsistent with the crystallographic complex. These findings validate the docking setup and justify its use for screening marine compounds in this study.

Following validation, marine compounds were screened and docked into the SHP2 allosteric tunnel using the same force field parameters. From the docking results, eighteen promising marine hits demonstrated superior docking scores (-7.855 to -5.773 kcal/mol) relative to *SHP099* (Table 1). These hits consistently occupied the allosteric pocket surrounded by residues Glu110, Arg111, Phe113, His114, Glu249, Glu250, and Thr253—residues known to stabilize the inactive conformation of SHP2.

Table 1. Docking scores, MM-PBSA, and RMSD profiles of docked marine hits compared with reference SHP099.

Sr. No.	Marine hits	Name	Source	Dock Score	MM-PBSA	RMSD
1	CMNPD23791	Hyrtioerectine E	Red Sea Marine Sponge Hyrtios [29]	-5.700 kcal/mol	-54.9 kcal/mol	0.118 Å
2	CMNPD15129	Hyrtioerectine A	Red Sea Sponge *Hyrtios erectus* [30]	-6.777 kcal/mol	-58.2 kcal/mol	0.136 Å
3	CMNPD25856	Pre-pseudomonine	*Pseudomonas fluorescens*	-5.757 kcal/mol	-53.3 kcal/mol	0.289 Å
4	CMNPD3610	Anguibactin	*Acinetobacter baumannii* [31]	-6.633 kcal/mol	-39.08 kcal/mol	0.277 Å
5	CMNPD7655	Oceanapamine	Philippine Sponge Oceanapia [32]	-6.207 kcal/mol	-37.05 kcal/mol	0.169 Å
6	CMNPD24248	Cladoloside D	Sea cucumber *Cladolabes schmeltzii* [33]	-5.949 kcal/mol	-31.88 kcal/mol	0.271 Å
7	CMNPD11182	Ceratinamine	Marine Sponge *Pseudoceratina purpurea* [34]	-6.401 kcal/mol	-29.30 kcal/mol	0.234 Å
8	CMNPD9170	Zoamide C	Philippine zoanthid *Parazoanthus [35]*	-6.228 kcal/mol	-49.18 kcal/mol	0.391 Å
9	CMNPD8539	Volutamide A	Atlantic bryozoan *Amathia convolute [36]*	-7.652 kcal/mol	-41.44 kcal/mol	0.178 Å
10	CMNPD29609	Terrazoanthine B	*Terrazoanthus onoi [37]*	-6.567 kcal/mol	-28.16 kcal/mol	0.279 Å
11	CMNPD11121	Naamine A	Calcareous sponge *leucetta chagosensis* [38]	-5.977 kcal/mol	-43.76 kcal/mol	0.174 Å
12	CMNPD6654	Prealmazole C	*Senegalese delesseriacean* seaweed [39]	-6.657 kcal/mol	-36.00 kcal/mol	0.157 Å

Sr. No.	Marine hits	Name	Source	Dock Score	MM-PBSA	RMSD
13	CMNPD29608	Terrazoanthine A	*Terrazoanthus onoi [37]*	-7.369 kcal/mol	-28.65 kcal/mol	0.312 Å
14	CMNPD7161	Lissoclin C	Tropical Lissoclinum [40]	-7.284 kcal/mol	-29.30 kcal/mol	0.310 Å
15	CMNPD25624	Pulmonarin B	Colonial Ascidian *Synoicum pulmonaria* [41]	-6.059 kcal/mol	-49.86 kcal/mol	0.188 Å
16	CMNPD9171	Zoamide D	Philippine *Parazoanthus* [35]	-5.773 kcal/mol	-28.50 kcal/mol	0.336 Å
17	CMNPD23466	Penilloid A	Marine-Derived Fungus *Penicillium* ZZ1750 [42]	-7.885 kcal/mol	-51.44 kcal/mol	0.089 Å
18	CMNPD11168	Cribrostatin 3	Blue Marine sponge *Cribrochalina* [43]	-6.577 kcal/mol	-32.52 kcal/mol	0.177 Å
19	Co-crystal	SHP099	PDB ID: 5EHR	-4.987 kcal/mol	-39.08 kcal/mol	0.420 Å

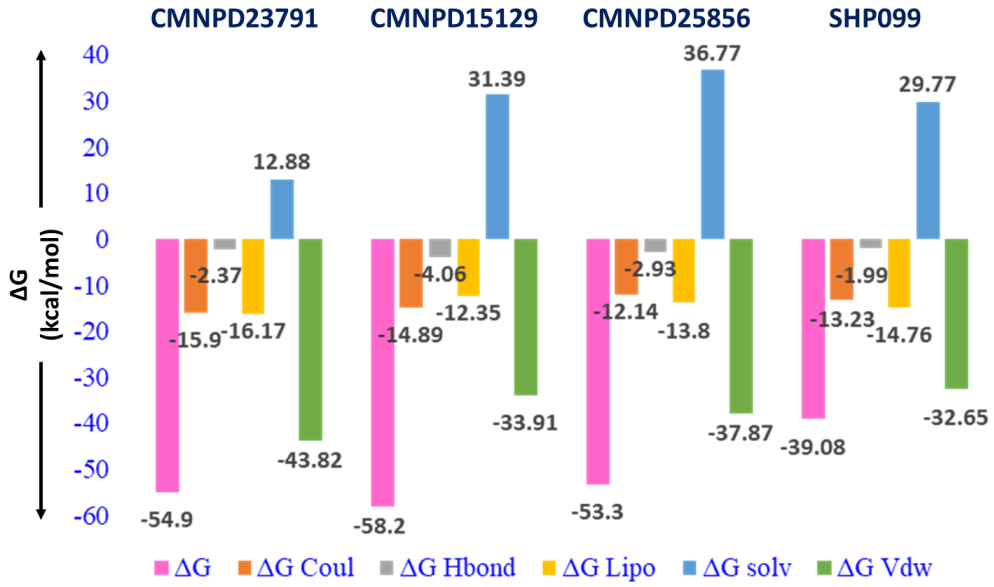

Figure 3. MM-PBSA and individual energetic components of top marine hits against SHP2. Units are in kcal/mol.

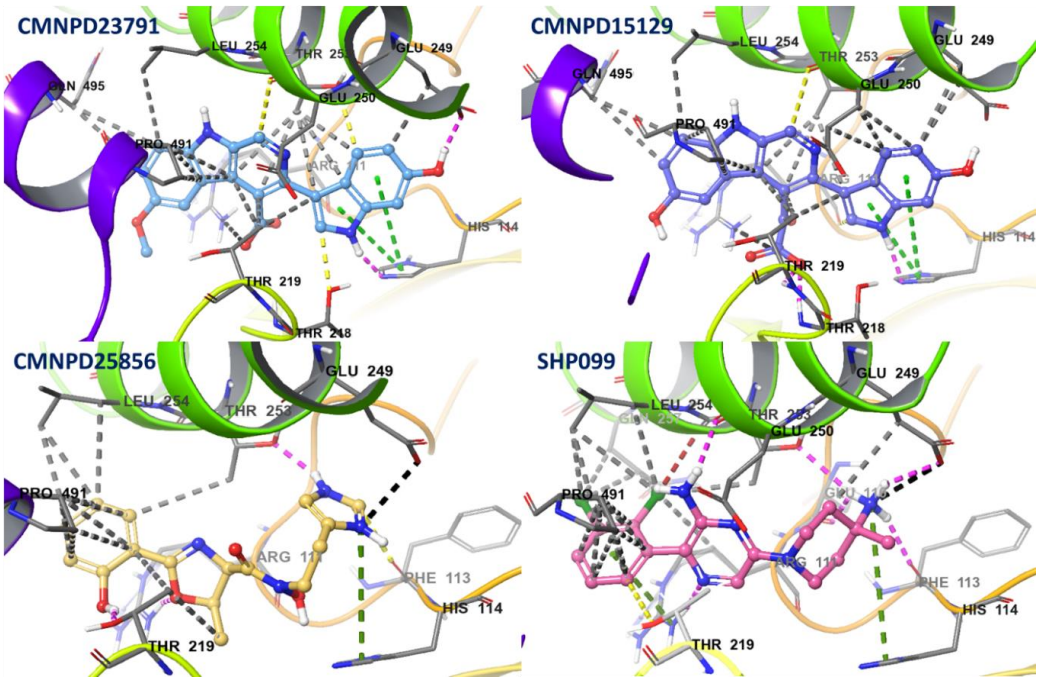

Figure 4. Molecular interactions of the top marine hits and the standard. Here, hydrogen bonding, aromatic-hydrogen bonds, π-π stacking, and hydrophobic interactions are colored in magenta, yellow, green, and grey, respectively.

To quantify the thermodynamic stability of these complexes, Molecular Mechanics Poisson-Boltzmann Surface Area (MM-PBSA) binding free-energy calculations were performed using 500 frames extracted from the last 20 ns of the equilibrated 100 ns MD trajectories. The convergence analysis confirmed minimal ΔG, deviations, ensuring the robustness of the computed values. Among the tested compounds, three marine hits — *CMNPD23791* (Hyrtioerectine E), *CMNPD15129* (Hyrtioerectine A), and *CMNPD25856* (pre-pseudomonine) exhibited the most favourable binding free energies of -54.9 kcal/mol, -58.2 kcal/mol, and -53.3 kcal/mol, respectively, surpassing the reference *SHP099* (-39.08 kcal/mol) (Figure 3). The interaction profiling of the best marine hits revealed a diverse and robust binding affinity landscape across key amino acid residues (Figure 4), which substantially contributed to their binding affinities (Table 2).

Table 2. Molecular interactions and per-residue energy decomposition of top marine hits

Marine Hits	Hydrogen bond	Aromatic H-bond	π- π stacking	Ionic	Hydrophobic
CMNPD23791	His114 (-43.01 kcal/mol), Glu249 (-61.33 kcal/mol)	Thr218 (-25.50 kcal/mol), Glu250 (-61.66 kcal/mol), Thr253 (-30.07 kcal/mol)	His114 (-43.01 kcal/mol)	Arg111 (-59.71 kcal/mol)	Thr219 (-22.56 kcal/mol), Leu254 (-37.34 kcal/mol), Pro491 (-16.80 kcal/mol), Gln495 (-74.01 kcal/mol)
CMNPD15129	His114 (-41.87 kcal/mol), Thr218 (-27.27 kcal/mol), Thr219 (-23.65 kcal/mol)	Arg111 (-59.21 kcal/mol), Glu250 (-61.03 kca/mol)	His114 (-41.87 kcal/mol)	Arg111 (-59.21)	Glu249 (-63.63 kcal/mol), Leu254 (-37.24 kcal/mol), Pro491 (-16.67 kcal/mol), Thr253 (-30.07 kcal/mol), Gln495 (-74.01 kcal/mol)
CMNPD25856	Arg111 (-59.15 kcal/mol), Thr219 (-26.16 kcal/mol), Thr253 (-32.75 kcal/mol)	Phe113 (-34.33 kcal/mol)	His114 (-43.76 kcal/mol)	Glu249 (-63.68)	Thr253 (-32.75 kcal/mol), Leu254 (-37.29 kcal/mol), Pro491 (-16.84 kcal/mol)
SHP099	Phe113 (-33.99 kcal/mol), Glu250 (-64.93 kcal/mol), Thr253 (-32.02 kcal/mol)	Thr219 (-24.09 kcal/mol)	His114 (-40.63 kcal/mol)	-	Glu110 (-57.35 kcal/mol), Thr253 (-32.02 kcal/mol), Leu254 (-37.95 kcal/mol), Gln257 (-78.77 kcal/mol), Pro491 (-17.60 kcal/mol)

3.3. Molecular dynamics simulation.

Molecular dynamics (MD) simulations were conducted to evaluate the stability, conformational flexibility, and dynamic behavior of the best-docked complexes over a 100 ns simulation period. The root mean square deviation (RMSD), root mean square fluctuation (RMSF), radius of gyration (Rg), and principal component analysis (PCA) were used to assess the dynamic behavior and structural properties of each complex. The RMSD reflects the overall conformational stability of a protein-ligand complex relative to its initial docked poses. All systems exhibited only minor fluctuations during the early stages of the simulation, indicating successful equilibration and ligand accommodation within the allosteric binding pocket. The average RMSD values for *CMNPD23791*, *CMNPD15129*, *CMNPD25856*, and the apo-form were 1.01 ± 0.14 Å, 1.05 ± 0.30 Å, 1.4 ± 0.33 Å, and 1.77 ± 0.19 Å, respectively (Figure 5).

RMSF analysis was performed to measure residue-level flexibility of the protein backbone, focusing on α-carbon atoms throughout the trajectory. Lower RMSF values indicate more rigid and stable regions. All complexes displayed similar RMSF patterns, with minimal fluctuations near the binding site residues. The average RMSF values of CMNPD23791, CMNPD15129, CMNPD25856, and the apo-form were 0.41 ± 0.36 Å, 0.55 ± 0.48 Å, 0.56 ± 0.49 Å, and 0.57 ± 0.52, respectively (Figure 6).

The compactness of the protein-ligand complexes, evaluated through the radius of gyration (Rg), further supported the structural stability observed across all systems. The Rg values for CMNPD23791, CMNPD15129, CMNPD25856, and the apo-form were 17.82 ± 0.13 Å, 17.63 ± 0.07 Å, 17.8 ± 0.103 Å, and 18.30 ± 0.10 Å, respectively, suggesting consistent structural compactness (Figure 7).

Principal component analysis (PCA) of the MD trajectories was carried out to examine the conformational space and collective motions of the α-carbon backbone. The two-dimensional projections of the first two principal components (PC1 and PC2) revealed compact, well-defined clusters for all systems Figure 8, indicating limited large-scale motions and stable conformational sampling. The MD results confirm that all three marine hits form highly stable complexes with SHP2, showing minimal conformational drift and strong structural integrity throughout the simulation.

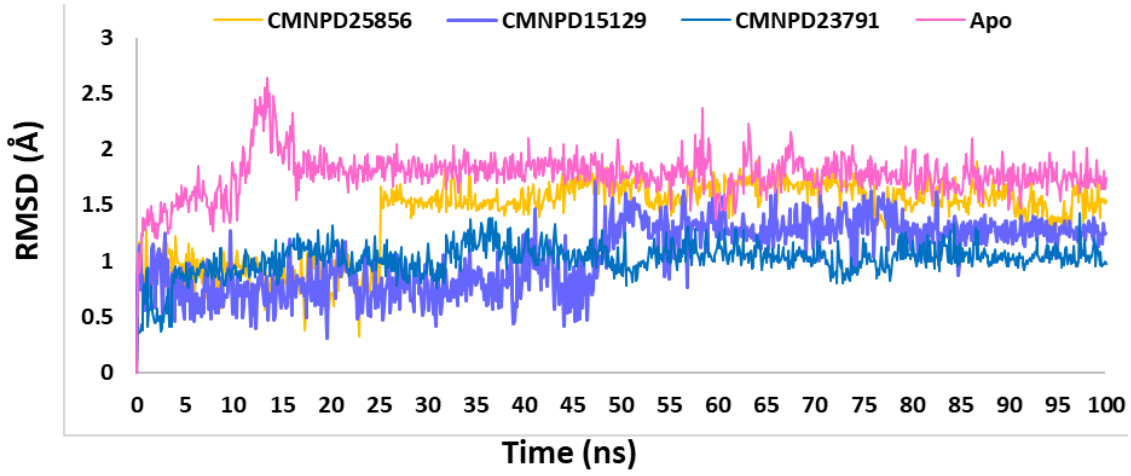

Figure 5. RMSD of top marine hits compared with the apo form during 100 ns MD simulations.

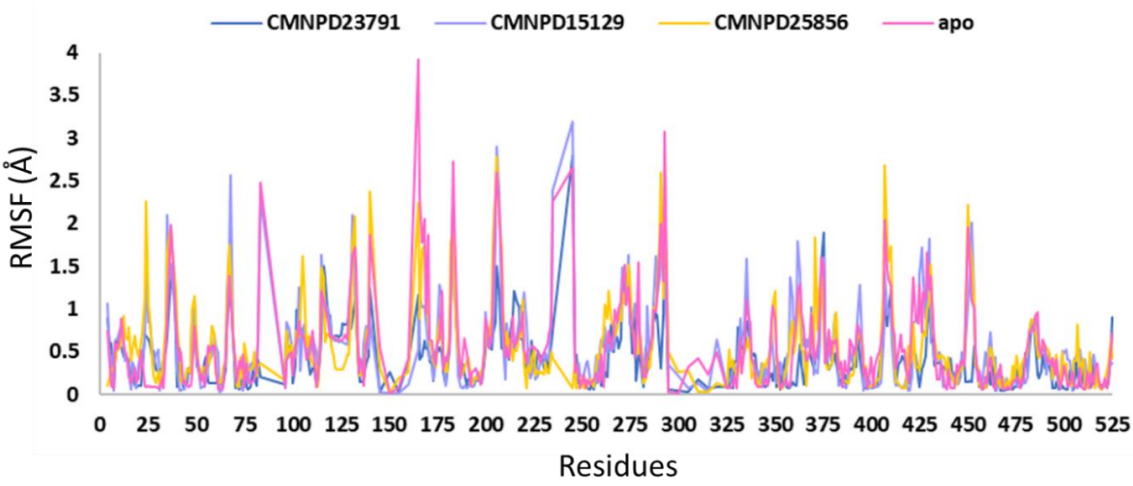

Figure 6. RMSF of top marine hits compared with the apo form during 100 ns MD simulations.

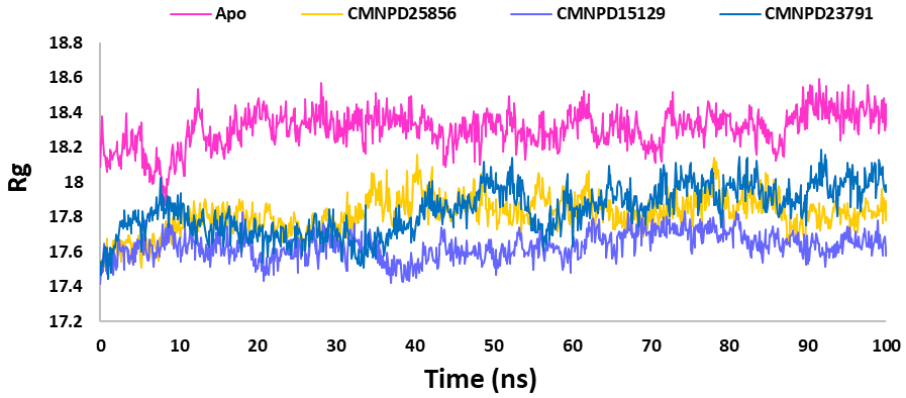

Figure 7. Radius of gyration (Rg) of top marine hits compared with the apo form during 100 ns MD simulations.

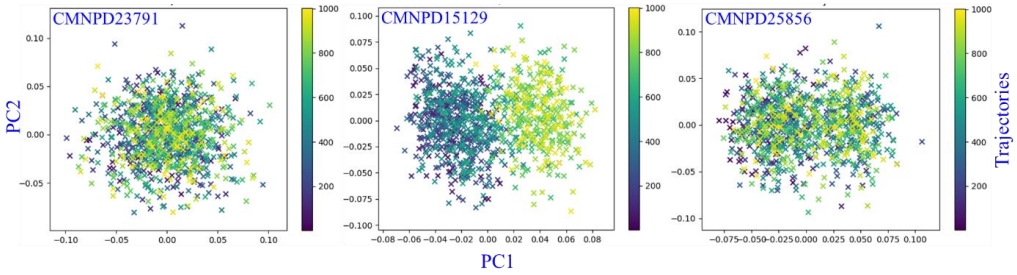

Figure 8. Principal Component Analysis (PCA) of top marine hits. The 2D projections of the first two principal components (PC1 vs. PC2) illustrate the conformational sampling of the α-carbon backbone.

3.4. Physicochemical and pharmacokinetic assessment.

The physicochemical and ADMET properties of the top marine hits SHP099 were evaluated to assess their drug-likeness and pharmacokinetic suitability (Table S1). All three marine hits complied with Lipinski's Rule of Five, showing molecular weights between 330 and 387 g/mol, LogP values within the acceptable range (1.1 to 4.3), and moderate polar surface areas (111–139 Å²), suggesting favorable oral bioavailability. All hits exhibited low aqueous solubility (–4.1 to –4.7), which is typical for hydrophobic marine alkaloids. Among them, CMNPD25856 demonstrated the best solubility profile and balanced lipophilicity, indicating potential for formulation optimization.

Toxicity predictions revealed that *CMNPD25856* had the lowest oral and cardiotoxic risks compared with *SHP099*, which exhibited higher toxicity indices. Conversely, *CMNPD23791* showed higher hepatotoxicity and carcinogenic potential, while *CMNPD15129* indicated possible drug-induced liver injury (DILI). Overall, *CMNPD25856* appeared to be the most favorable candidate, balancing drug-likeness, safety, and predicted pharmacokinetic properties.

3.5. Discussions.

The identified marine hits revealed significantly higher binding affinities and greater complex stability than the reference *SHP099* and other reported SHP2 allosteric inhibitors. The MM-PBSA results showed ΔGbind values for CMNPD23791 (Hyrtioerectine E), CMNPD15129 (Hyrtioerectine A), and CMNPD25856 (pre-pseudomonine) relative to *SHP099*. These values suggest a stronger and more stable interaction profile. The predicted affinities were also comparable, indicating that the marine hits exhibit superior thermodynamic stability. Structurally, *SHP099* and its analogs are characterized by rigid tricyclic frameworks

that interact mainly through π–π stacking and hydrogen bonds at the central tunnel. In contrast, Hyrtioerectine A and E possess extended aromatic systems with halogen substituents that enable broader van der Waals and π-cation contacts with key residues Arg111, Phe113, and Glu249. This expanded interaction surface enhances conformational adaptability and improves energetic stability. Pre-pseudomonine, with its flexible heterocyclic core, maintained persistent hydrogen bonding with His114, Glu249, and Thr253, reinforcing the complex during the 100 ns simulation. The dynamic stability of these complexes was confirmed by low RMSD and compact Rg profiles, signifying minimal structural deviation and effective equilibration. The energy decomposition analysis indicated that van der Waals and hydrophobic contributions were dominant, implying that the marine hits engage deeper non-polar regions of the allosteric tunnel than conventional inhibitors. Such stable hydrophobic embedding is often associated with enhanced inhibition efficiency. ADMET analysis satisfied Lipinski's Rule of Five, confirming acceptable physicochemical profiles. Marine hits showed optimal hydrophobicity, moderate solubility, and the lowest predicted cardiotoxicity, outperforming *SHP099*, which exhibited higher hepatotoxic and genotoxic probabilities. Hyrtioerectine A demonstrated moderate oral absorption but a higher potential for drug-induced liver injury, while Hyrtioerectine E showed elevated carcinogenicity risk linked to its high lipophilicity.

While we truly acknowledge the limitations of our study, as the absence of alchemical free energy studies and biological evaluation based on our computational findings, we aimed to accomplish follow-up, cell-based, target-based, and micro-dosing studies with a potential implication for cancer therapy, which are still underway, and the results are anticipated to be published in the follow-up studies.

4. Conclusions

This study employed an integrated computational approach combining receptor-guided pharmacophore modeling, molecular docking, MM-PBSA energy profiling, and molecular dynamics simulations to identify marine allosteric SHP2 inhibitors. Among the screened compounds, *CMNPD23791* (Hyrtioerectine E), *CMNPD15129* (Hyrtioerectine A), and *CMNPD25856* (pre-pseudomonine) exhibited superior binding free energies and strong interactions with key residues at the SHP2 allosteric pocket compared with the reference *SHP099*. The molecular dynamics trajectories confirmed high structural stability and minimal backbone deviation, while ADMET predictions indicated acceptable physicochemical and safety profiles. These findings collectively indicate that the identified marine compounds may serve as lead scaffolds for next-generation SHP2 inhibitors, offering potential improvements in both affinity and predicted safety relative to existing clinical candidates. Their distinct structural motifs and favorable binding energetics underscore their translational promise for the development of novel therapeutics targeting SHP2-driven cancers. However, this study is limited by the absence of experimental validation. Future work will focus on experimental confirmation of SHP2 inhibition, cytotoxicity assays, and structural optimization to further enhance therapeutic applicability.

Author Contributions

Conceptualization, S.K.P. and J.P.; methodology, P.S.; formal analysis, P.S.; investigation, P.S.; writing—original draft preparation, P.S.; writing—review and editing, S.K.P. and J.P.;

supervision, S.K.P. and J.P. All authors have read and agreed to the published version of the manuscript.

Institutional Review Board Statement

Not applicable.

Informed Consent Statement

Not applicable.

Data Availability Statement

Data supporting the findings of this study are available upon reasonable request from the corresponding author.

Funding

This research received no external funding.

Acknowledgments

All authors gratefully acknowledged Bioinformatics Resources and Advanced Facility (BRAF) Pune, implemented by the CDAC and supported by the Ministry of Electronics and Information Technology (MeITY) and the Department of Science and Technology (DST), India. The authors acknowledge the Amity Institute of Pharmacy, Amity University Uttar Pradesh, Lucknow Campus, for allowing them to conduct this research.

Conflicts of Interest

The authors declare no conflict of interest.

Abbreviations

The following abbreviations are used in this manuscript:

Abbreviation	Definition
Å	Angstrom
ADMET	Absorption, Distribution, Metabolism, Excretion, and Toxicity
CMNPD	Comprehensive Marine Natural Product Database
DILI	Drug-Induced Liver Injury
MDS	Molecular Dynamics Simulation
MM-PBSA	Molecular Mechanics Poisson-Boltzmann Surface Area
PAINS	Pan Assay Interference
PCA	Principal Component Analysis
PDB	Protein Data Bank
PRED	Per-Residue Energy Decomposition
Rg	Radius of Gyration
RMSD	Root Mean Square Deviation
RMSF	Root Mean Square Fluctuation
SHP2	Src homology-2-containing protein tyrosine phosphatase

References

1. Song, Y.; Wang, S.; Zhao, M.; Yang, X.; Yu, B. Strategies Targeting Protein Tyrosine Phosphatase SHP2 for Cancer Therapy. *J. Med. Chem.* **2022**, *65*, 3066-3079, https://doi.org/10.1021/acs.jmedchem.1c02008.
2. Stanford, S.M.; Bottini, N. Targeting protein phosphatases in cancer immunotherapy and autoimmune disorders. *Nat. Rev. Drug Discov.* **2023**, *22*, 273-294, https://doi.org/10.1038/s41573-022-00618-w.
3. Ostman, A.; Hellberg, C.; Böhmer, F.D. Protein-tyrosine phosphatases and cancer. *Nat. Rev. Cancer* **2006**, *6*, 307-320, https://doi.org/10.1038/nrc1837.
4. Tajan, M.; de Rocca Serra, A.; Valet, P.; Edouard, T.; Yart, A. SHP2 sails from physiology to pathology. *Eur. J. Med. Genet.* **2015**, *58*, 509-525, https://doi.org/10.1016/j.ejmg.2015.08.005.
5. Sodir, N.M.; Pathria, G.; Adamkewicz, J.I.; Kelley, E.H.; Sudhamsu, J.; Merchant, M.; Chiarle, R.; Maddalo, D. SHP2: A Pleiotropic Target at the Interface of Cancer and Its Microenvironment. *Cancer Discov.* **2023**, *13*, 2339-2355, https://doi.org/10.1158/2159-8290.Cd-23-0383.
6. Scheiter, A.; Lu, L.C.; Gao, L.H.; Feng, G.S. Complex Roles of PTPN11/SHP2 in Carcinogenesis and Prospect of Targeting SHP2 in Cancer Therapy. *Annu. Rev. Cancer Biol.* **2024**, *8*, 15-33, https://doi.org/10.1146/annurev-cancerbio-062722-013740.
7. Chen, L.; Sung, S.S.; Yip, M.L.; Lawrence, H.R.; Ren, Y.; Guida, W.C.; Sebti, S.M.; Lawrence, N.J.; Wu, J. Discovery of a novel shp2 protein tyrosine phosphatase inhibitor. *Mol. Pharmacol.* **2006**, *70*, 562-570, https://doi.org/10.1124/mol.106.025536.
8. Hellmuth, K.; Grosskopf, S.; Lum, C.T.; Würtele, M.; Röder, N.; von Kries, J.P.; Rosario, M.; Rademann, J.; Birchmeier, W. Specific inhibitors of the protein tyrosine phosphatase Shp2 identified by high-throughput docking. *Proc. Natl. Acad. Sci. USA* **2008**, *105*, 7275-7280, https://doi.org/10.1073/pnas.0710468105.
9. Yuan, X.; Bu, H.; Zhou, J.; Yang, C.Y.; Zhang, H. Recent Advances of SHP2 Inhibitors in Cancer Therapy: Current Development and Clinical Application. *J. Med. Chem.* **2020**, *63*, 11368-11396, https://doi.org/10.1021/acs.jmedchem.0c00249.
10. Chen, Y.-N.P.; LaMarche, M.J.; Chan, H.M.; Fekkes, P.; Garcia-Fortanet, J.; Acker, M.G.; Antonakos, B.; Chen, C.H.-T.; Chen, Z.; Cooke, V.G. Allosteric inhibition of SHP2 phosphatase inhibits cancers driven by receptor tyrosine kinases. *Nature* **2016**, *535*, 148-152, https://doi.org/10.1038/nature18621.
11. LaMarche, M.J.; Acker, M.; Argintaru, A.; Bauer, D.; Boisclair, J.; Chan, H.; Chen, C.H.-T.; Chen, Y.-N.; Chen, Z.; Deng, Z. Identification of TNO155, an allosteric SHP2 inhibitor for the treatment of cancer. *J. Med. Chem.* **2020**, *63*, 13578-13594, https://doi.org/10.1021/acs.jmedchem.0c01170.
12. Shen, D.; Chen, W.; Zhu, J.; Wu, G.; Shen, R.; Xi, M.; Sun, H. Therapeutic potential of targeting SHP2 in human developmental disorders and cancers. *Eur. J. Med. Chem.* **2020**, *190*, 112117, https://doi.org/10.1016/j.ejmech.2020.112117.
13. Taylor, A.M.; Williams, B.R.; Giordanetto, F.; Kelley, E.H.; Lescarbeau, A.; Shortsleeves, K.; Tang, Y.; Walters, W.P.; Arrazate, A.; Bowman, C. Identification of GDC-1971 (RLY-1971), a SHP2 inhibitor designed for the treatment of solid tumors. *J. Med. Chem.* **2023**, *66*, 13384-13399, https://doi.org/10.1021/acs.jmedchem.3c00483.
14. Drilon, A.; Sharma, M.R.; Johnson, M.L.; Yap, T.A.; Gadgeel, S.; Nepert, D.; Feng, G.; Reddy, M.B.; Harney, A.S.; Elsayed, M. SHP2 inhibition sensitizes diverse oncogene-addicted solid tumors to re-treatment with targeted therapy. *Cancer Discov.* **2023**, *13*, 1789-1801, https://doi.org/10.1158/2159-8290.Cd-23-0361.
15. Brana, I.; Shapiro, G.; Johnson, M.L.; Yu, H.A.; Robbrecht, D.; Tan, D.S.-W.; Siu, L.L.; Minami, H.; Steeghs, N.; Hengelage, T. Initial results from a dose finding study of TNO155, a SHP2 inhibitor, in adults with advanced solid tumors. *J. Clin. Oncol.* **2021**, *39*, 15, https://doi.org/10.1200/JCO.2021.39.15_suppl.3005.
16. Veeresham, C. Natural products derived from plants as a source of drugs. *J. Adv. Pharm. Technol. Res.* **2012**, *3*, 200-201, https://doi.org/10.4103/2231-4040.104709.
17. Ganesan, A. The impact of natural products upon modern drug discovery. *Curr. Opin. Chem. Biol.* **2008**, *12*, 306-317, https://doi.org/10.1016/j.cbpa.2008.03.016.
18. Lee, M.L.; Schneider, G. Scaffold architecture and pharmacophoric properties of natural products and trade drugs: application in the design of natural product-based combinatorial libraries. *J. Comb. Chem.* **2001**, *3*, 284-289, https://doi.org/10.1021/cc000097l.
19. Carlsson, J.; Luttens, A. Structure-based virtual screening of vast chemical space as a starting point for drug discovery. *Curr. Opin. Struct. Biol.* **2024**, *87*, 102829, https://doi.org/10.1016/j.sbi.2024.102829.

20. Shoichet, B.K. Virtual screening of chemical libraries. *Nature* **2004**, *432*, 862-865, https://doi.org/10.1038/nature03197.
21. Lu, J.; Yu, D.; Li, H.; Qin, P.; Chen, H.; Chen, L. Promising natural products targeting protein tyrosine phosphatase SHP2 for cancer therapy. *Phytother. Res.* **2025**, *39*, 1735-1757, https://doi.org/10.1002/ptr.8185.
22. Liang, W.; Krabill, A.D.; Gallagher, K.S.; Muli, C.; Qu, Z.; Trader, D.; Zhang, Z.-Y.; Dai, M. Natural product-inspired molecules for covalent inhibition of SHP2 tyrosine phosphatase. *Tetrahedron* **2024**, *156*, 133918, https://doi.org/10.1016/j.tet.2024.133918.
23. Lyu, C.; Chen, T.; Qiang, B.; Liu, N.; Wang, H.; Zhang, L.; Liu, Z. CMNPD: a comprehensive marine natural products database towards facilitating drug discovery from the ocean. *Nucleic Acids Res.* **2021**, *49*, D509-D515, https://doi.org/10.1093/nar/gkaa763.
24. Fu, L.; Shi, S.; Yi, J.; Wang, N.; He, Y.; Wu, Z.; Peng, J.; Deng, Y.; Wang, W.; Wu, C. ADMETlab 3.0: an updated comprehensive online ADMET prediction platform enhanced with broader coverage, improved performance, API functionality and decision support. *Nucleic Acids Res.* **2024**, *52*, W422-W431, https://doi.org/10.1093/nar/gkae236.
25. Sunseri, J.; Koes, D.R. Pharmit: interactive exploration of chemical space. *Nucleic Acids Res.* **2016**, *44*, W442-448, https://doi.org/10.1093/nar/gkw287.
26. Kabier, M.; Gambacorta, N.; Trisciuzzi, D.; Kumar, S.; Nicolotti, O.; Mathew, B. MzDOCK: A free ready-to-use GUI-based pipeline for molecular docking simulations. *J. Comput. Chem.* **2024**, *45*, 1980-1986, https://doi.org/10.1002/jcc.27390.
27. Kumari, R.; Kumar, R.; Lynn, A. g_mmpbsa—A GROMACS Tool for High-Throughput MM-PBSA Calculations. *J. Chem. Inf. Model* **2014**, *54*, 1951-1962, https://doi.org/10.1021/ci500020m.
28. Bowers, K.J.; Chow, E.; Xu, H.; Dror, R.O.; Eastwood, M.P.; Gregersen, B.A.; Klepeis, J.L.; Kolossvary, I.; Moraes, M.A.; Sacerdoti, F.D.; Salmon, J.K.; Shan, Y.; Shaw, D.E. Scalable algorithms for molecular dynamics simulations on commodity clusters. Proceedings of the 2006 ACM/IEEE conference on Supercomputing, Tampa, Florida, **2006**; pp. 84–es, https://doi.org/10.1145/1188455.1188544.
29. Youssef, D.T.; Shaala, L.A.; Asfour, H.Z. Bioactive compounds from the Red Sea marine sponge Hyrtios species. *Mar. Drugs* **2013**, *11*, 1061-1070, https://doi.org/10.3390/md11041061.
30. Youssef, D.T.A. Hyrtioerectines A−C, Cytotoxic Alkaloids from the Red Sea Sponge Hyrtios erectus. *J. Nat. Prod.* **2005**, *68*, 1416-1419, https://doi.org/10.1021/np050142c.
31. Lee, H.; Song, W.Y.; Kim, M.; Lee, M.W.; Kim, S.; Park, Y.S.; Kwak, K.; Oh, M.H.; Kim, H.J. Synthesis and Characterization of Anguibactin To Reveal Its Competence To Function as a Thermally Stable Surrogate Siderophore for a Gram-Negative Pathogen, Acinetobacter baumannii. *Org. Lett.* **2018**, *20*, 6476-6479, https://doi.org/10.1021/acs.orglett.8b02789.
32. Boyd, K.G.; Harper, M.K.; Faulkner, D.J. Oceanapamine, a Sesquiterpene Alkaloid from the Philippine Sponge Oceanapia sp. *J. Nat. Prod.* **1995**, *58*, 302-305, https://doi.org/10.1021/np50116a027.
33. Silchenko, A.S.; Kalinovsky, A.I.; Avilov, S.A.; Andryjaschenko, P.V.; Dmitrenok, P.S.; Yurchenko, E.A.; Ermakova, S.P.; Malyarenko, O.S.; Dolmatov, I.Y.; Kalinin, V.I. Cladolosides C(4), D(1), D(2), M, M(1), M(2), N and Q, new triterpene glycosides with diverse carbohydrate chains from sea cucumber Cladolabes schmeltzii. An uncommon 20,21,22,23,24,25,26,27-okta-nor-lanostane aglycone. The synergism of inhibitory action of non-toxic dose of the glycosides and radioactive irradiation on colony formation of HT-29 cancer cells. *Carbohydr. Res.* **2018**, *468*, 36-44, https://doi.org/10.1016/j.carres.2018.08.003.
34. Tsukamoto, S.; Kato, H.; Hirota, H.; Fusetani, N. Ceratinamine: An Unprecedented Antifouling Cyanoformamide from the Marine Sponge Pseudoceratina purpurea. *J. Org. Chem.* **1996**, *61*, 2936-2937, https://doi.org/10.1021/jo9602884.
35. D'Ambrosio, M.; Roussis, V.; Fenical, W.J.T.l. Zoamides, A.D. New marine zoanthoxanthin class alkaloids from an encrusting Philippine Parazoanthus sp. *Tetrahedron Lett.* **1997**, *38*, 717-720, https://doi.org/10.1016/S0040-4039(96)02423-9.
36. Montanari, A.M.; Fenical, W.; Lindquist, N.; Lee, A.Y.; Clardy, J.J.T. Volutamides AE, halogenated alkaloids with antifeedant properties from the Atlantic bryozoan Amathia convoluta. *Tetrahedron* **1996**, *52*, 5371-5380, https://doi.org/10.1016/0040-4020(96)00188-3.
37. Guillen, P.O.; Jaramillo, K.B.; Genta-Jouve, G.; Sinniger, F.; Rodriguez, J.; Thomas, O.P.J.O.L. Terrazoanthines, 2-aminoimidazole alkaloids from the Tropical Eastern Pacific zoantharian Terrazoanthus onoi. *Org. Lett.* **2017**, *19*, 1558-1561, https://doi.org/10.1021/acs.orglett.7b00369.

38. Carmely, S.; Kashman, Y.J.T.l. Naamines and naamidines, novel imidazole alkaloids from the calcareous sponge Leucetta chagosensis. *Tetrahedron Lett.* **1987**, *28*, 3003-3006, https://doi.org/10.1016/S0040-4039(00)96268-3.
39. Guella, G.; Mancini, I.; Pietra, F.J.H.c.a. Almazole C, a new indole alkaloid bearing an unusually 2, 5-disubstituted oxazole moiety, and its putative biogenetic peptidic precursors, from a senegalese delesseriacean seaweed. *Helv. Chim. Acta* **1994**, *77*, 1999-2006, https://doi.org/10.1002/hlca.19940770726.
40. Searle, P.A.; Molinski, T.F.J.T.J.O.O.C. Five new alkaloids from the tropical ascidian, Lissoclinum sp. lissoclinotoxin A is chiral. *J. Org. Chem.* **1994**, *59*, 6600-6605, https://doi.org/10.1021/jo00101a018.
41. Tadesse, M.; Svenson, J.; Sepčić, K.; Trembleau, L.; Engqvist, M.; Andersen, J.H.; Jaspars, M.; Stensvåg, K.; Haug, T.J.J.o.n.p. Isolation and synthesis of pulmonarins A and B, acetylcholinesterase inhibitors from the colonial ascidian Synoicum pulmonaria. *J. Nat. Prod.* **2014**, *77*, 364-369, https://doi.org/10.1021/np401002s.
42. Yong, K.; Kaleem, S.; Ma, M.; Lian, X.; Zhang, Z. Antiglioma Natural Products from the Marine-Associated Fungus Penicillium sp. ZZ1750. *Molecules* **2022**, *27*, 7099, https://doi.org/10.3390/molecules27207099.
43. Pettit, G.R.; Knight, J.C.; Collins, J.C.; Herald, D.L.; Pettit, R.K.; Boyd, M.R.; Young, V.G. Antineoplastic agents 430. Isolation and structure of cribrostatins 3, 4, and 5 from the republic of maldives cribrochalina species. *J. Nat. Prod.* **2000**, *63*, 793-798, https://doi.org/10.1021/np990618q.

Publisher's Note & Disclaimer

Supplementary information

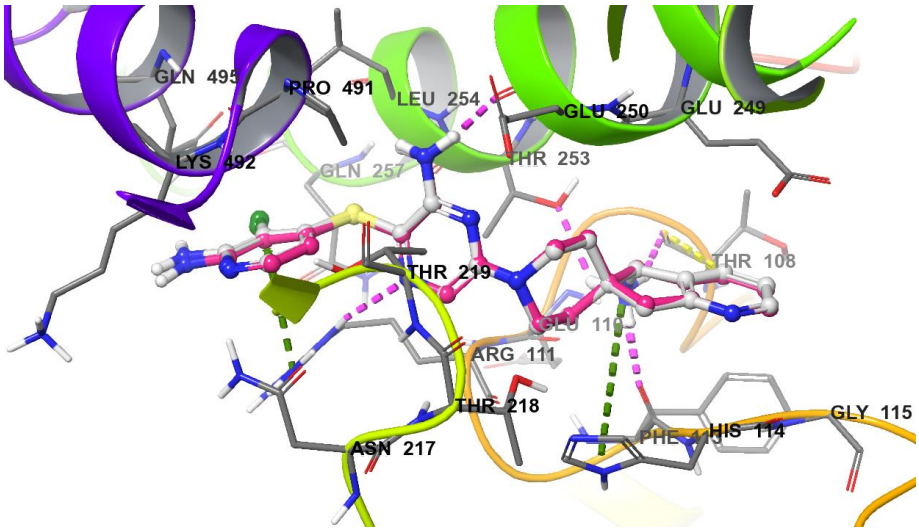

Figure S1. Docking validation of co-crystallized inhibitor SHP099. The experimental SHP099 and re-docked SHP099 are colored in white and magenta, respectively. Hydrogen bonding and π-π stacking are shown in magenta and dark green dashed lines, respectively.

Table S1. Physicochemical and ADMET profiling of top marine hits and standard SHP099. The predictive toxicity values range from 0 to 1, with 0 representing lower toxicity and 1 representing higher toxicity.

Sr. No.	Parameters	CMNPD25856	CMNPD15129	CMNPD23791	SHP099
1	Mol Wt. (g/mol)	330.34	387.35	373.37	352.27
2	HBD	3.00	5.00	4.00	2.00
3	HBA	6.00	5.00	4.00	5.00
4	Rot. Bonds	6,00	3.0	3.0	2.0
5	TPSA ($Å^{2)}$	111.04	139.30	111.23	81.06
6	Solubility	-4.758	-4.155	-4.451	-4.058
7	$LogP_{o/w}$	1.11	3.54	4.28	3.35
8	Caco-2 (cm/sec)	-5.66	-5.537	-5.359	-5.245
9	PPB	73.43	90.808	97.018	79.532
10	Clearance	4.421	0.49	0.872	4.949
11	Half-life (hrs)	1.626	1.533	1.346	1.342
12	Oral toxicity	0.352	0.549	0.555	0.663
13	hERG Blockers	0.05	0.143	0.268	0.604
14	DILI	0.58	0.949	0.976	0.819
15	Carcinogenicity	0.403	0.45	0.687	0.664
16	Eye irritation	0.012	0.947	0.929	0.104
17	Mutagenicity	0.56	0.586	0.712	0.458
18	Hepatotoxicity	0.803	0.766	0.719	0.869
19	Nephrotoxicity	0.925	0.809	0.928	0.885
20	Hematotoxicity	0.655	0.388	0.504	0.717
21	Genotoxicity	1.0	0.985	0.917	0.966
22	Neurotoxicity	0.836	0.665	0.789	0.941